JOURNAL OF MATERIALS SCIENCE 20 (1985) 4459–4464

Residual stresses of thin, short rectangular plates

ARSAVIR T. ANDONIAN,* STEVEN DANYLUK
Department of Civil Engineering, Mechanics and Metallurgy, University of Illinois at Chicago, Box 4348, Chicago, Illinois 60680, USA

The analysis of the residual stresses in thin, short rectangular plates is presented. The analysis is used in conjunction with a shadow Moiré interferometry technique by which residual stresses are obtained over a large spatial area from a strain measurement. The technique and analysis are applied to a residual stress measurement of polycrystalline silicon sheet grown by the edge-defined film growth technique.

1. Introduction

Residual stresses are an important contributing cause to the buckling and fracture of engineering components. Out-of-plane residual stresses result in distortion and, in some instances, may lead to fracture. The distortion provides evidence of the existence of these stresses and may be used to determine whether the component is acceptable in a particular design application. In-plane residual stresses, on the other hand, are insidious since they are not visually detectable but can promote slow crack growth as in the stress-corrosion cracking of metals, or fast fracture as in the brittle catastrophic fracture of ceramics and glasses. There are a number of destructive and non-destructive methods [1–9] for measuring residual stresses, and a number of these have been directed at the detection of in-plane residual stresses. The two most widely used non-destructive techniques are the X-ray and the hole-drilling strain gauge technique. In the X-ray technique, X-ray photons are diffracted from the top few micrometres of a millimetre-square area of a sample surface and the widths of selected diffraction peaks are analysed. The spread in the peak is due to lattice strain imposed by the residual stresses. In the hole-drilling strain gauge method, a special rosette strain gauge is bonded to the surface and a small hole is drilled through the centre of the gauge. The resulting change in strain around the hole due to the residual stress relaxation is measured. In both of these techniques, it is inconvenient to measure the strains through the thickness or over large areas of the component.

In this paper we report on the application of an interferometry technique for the measurement of in-plane residual stresses. The technique has several advantages over the methods described above. It is simple and straightforward, and the sensitivity may be adjusted to suit experimental needs; it is non-destructive and suitable to provide strains over large spatial areas.

Although the technique can be applied to any thin ceramic or metal plate whose width is of the order of the length, it is specialized here to the measurement of thin short rectangular silicon plates that have non-polished but parallel surfaces. The silicon, used here as a typical prototypic material, is flexed in a four-point bend fixture and the strains imposed by these applied loads are measured from interferograms produced by an optical grating [10]. The residual stresses are determined from an analysis of the expected deflection and curvature. A sample experimental measurement of a silicon plate is presented.

**Present address*: Goodyear Tire and Rubber Company, Akron, Ohio, USA.

0022–2461/85 $03.00 + .12 © *1985 Chapman and Hall Ltd.*

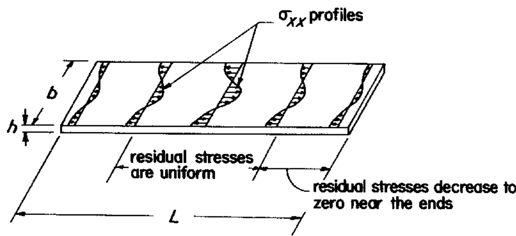

Figure 1 A schematic diagram of a short, thin unbuckled plate containing a heterogeneous in-plane residual stress distribution σ_x. The stress decreases to zero at the ends of the plate.

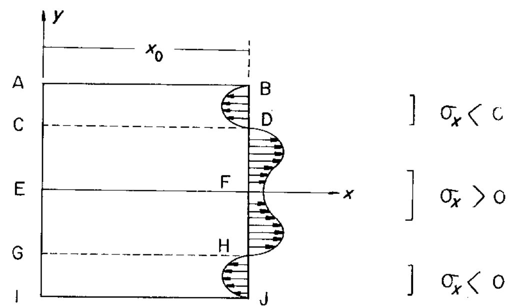

Figure 2 Schematic representation of the in-plane residual stresses along an arbitrary transverse section of the plate.

2. Analysis

Assume a flat (non-buckled) plate of uniform thickness h, of width b one-half the length, and no body forces or out-of-plane residual stresses. Fig. 1 shows a schematic diagram of the plate and a possible variation of the in-plane residual stresses σ_{xx} that are uniform in the centre and decrease to zero at the two ends. Fig. 2 shows a schematic diagram of the possible state of in-plane residual stress at a location x_0. This stress must decrease to zero at $x = 0$ since this surface is traction-free. This residual stress is necessarily heterogeneous since it decreases to zero at the ends. Fig. 3 shows a possible variation of shear flow Q along the longitudinal sections (parallel to the x–z axis) where the sign of the residual stress changes.

The variation of σ_{xx} along the width identified in Fig. 2 necessitates the use of separate models for the different states of stress, and the two formulations below include these two cases when bending moments are applied. We use this analysis to compare with experimental results.

2.1. Case I: rectangular plate under bending, in-plane tension and side shear

If the plate between Points C and G in Fig. 3 was subjected to out-of-plane bending, the mid-portion could be treated as a rectangular plate under bending, in-plane tension and side shear. A narrow plate element of width Δy is shown in Fig. 4 for a short plate. This diagram includes the free end where the stress residual P is zero and a shear flow q $(= \tau_{xz} h \, \mathrm{d}s)$ is present to compensate for the decrease of P from the position x_0 to the free end. The variation of shear flow q is assumed, for simplicity, to be linear over the major portion of the plate and decreases to zero near the ends since these are traction-free. This variation in shear flow is shown in Fig. 5 for a plate of length L. The shear flow q (not drawn to scale in this figure) reaches a maximum value and then falls to zero within a distance of the order of the thickness of the plate.

The shear flow not near the ends shown in Fig. 5 can be expressed as

$$q \cong K\left(\frac{L}{2} - x\right) \tag{1}$$

where K represents the change in shear flow per unit length. The applied bending moment M is distributed along the length of the plate and at x_0 the bending moment is M'.

If the deflection along the plate is approximated as

$$w = Ax^2 + Bx + C$$

and the boundary conditions are given as

$$[x = 0, w = 0]; \qquad [x = L, w = 0]$$

then

$$w = A(x^2 - Lx) \tag{2}$$

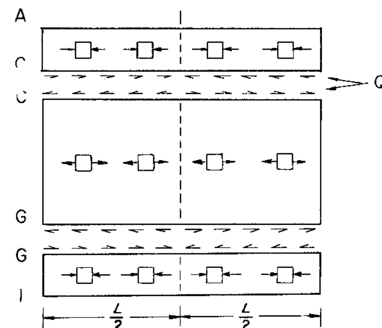

Figure 3 Schematic representation of the residual stresses along the length of the plate and the shear flow on longitudinal sections where the sign of residual stress changes.

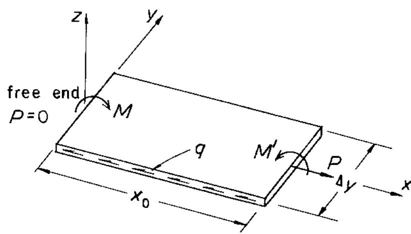

Figure 4 A narrow plate element of width Δy. This element includes the end ($x = 0$) where $P = 0$.

Considering angular equilibrium,

$$M' = M - Pw + M_q \qquad (3)$$

where

$$M_q = 2\int_0^{x_0} qw\,\mathrm{d}x \qquad (4)$$

From linear equilibrium the stress residual in the x-direction can be written as

$$P = 2\int_0^{x_0} q\,\mathrm{d}x \qquad (5)$$

Substituting Equation 1 into Equation 5,

$$P = 2\int_0^{x_0} K\left(\frac{L}{2} - x\right)\mathrm{d}x$$

Solving for K,

$$K = \frac{P}{Lx_0 - x_0^2} \qquad (6)$$

and comparing Equations 1 and 6 we get

$$q = \frac{P}{x_0^2 - Lx_0}\left(x - \frac{L}{2}\right) \qquad (7)$$

Substituting Equations 2 and 7 into Equation 4,

$$M_q = 2\int_0^{x_0}\left(\frac{P}{x_0^2 - Lx_0}\right) \times \left(x - \frac{L}{2}\right) A(x^2 - Lx)\,\mathrm{d}x$$

or

$$M_q = \frac{AP}{2}(x_0^2 - Lx_0) \qquad (8)$$

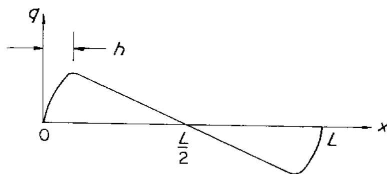

Figure 5 Shear flow variation along a longitudinal cut of the plate shown in Fig. 4.

Substituting Equation 8 into Equation 3,

$$M' = M - Pw + \frac{AP}{2}(x_0^2 - Lx_0) \qquad (9)$$

Finally, assuming small deflections and utilizing the relation for plate curvature we get

$$\frac{1}{\varrho} = \frac{\mathrm{d}^2 w}{\mathrm{d}x^2} = \frac{M'}{D}$$

where

$$D = \frac{Eh^3 b}{12(1 - \nu^2)}$$

and h = plate thickness, b = plate width, E = modulus of elasticity and ν = Poisson's ratio. The governing equation for Case I can then be written as

$$\frac{\mathrm{d}^2 w}{\mathrm{d}x^2} = \frac{M}{D} - \frac{P}{D}w + \frac{AP}{2D}(x_0^2 - Lx_0) \qquad (10)$$

where $(\mathrm{d}^2 w/\mathrm{d}x^2) = 2A$ (to be determined experimentally), M = applied moment (known) and w = measured deflection at x_0.

2.2. Case II: rectangular plate under bending, in-plane compression and side shear

The state of loading in Regions A–C or G–I (Fig. 3) is one of in-plane compression, side shear and bending and is shown in Fig. 6. Similar to Case I, the angular equilibrium can be expressed as

$$M' = M + Pw - M_q \qquad (11)$$

Substituting Equation 8 into Equation 11,

$$M' = M + Pw - \frac{AP}{2}(x_0^2 - Lx_0) \qquad (12)$$

and the governing equation is

$$\frac{\mathrm{d}^2 w}{\mathrm{d}x^2} = \frac{M}{D} + \frac{P}{D}w - \frac{AP}{2D}(x_0^2 - Lx_0) \qquad (13)$$

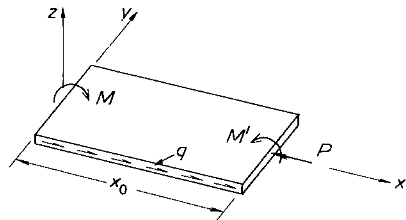

Figure 6 State of stress in Case II. (M, M', and P are described in Fig. 5.)

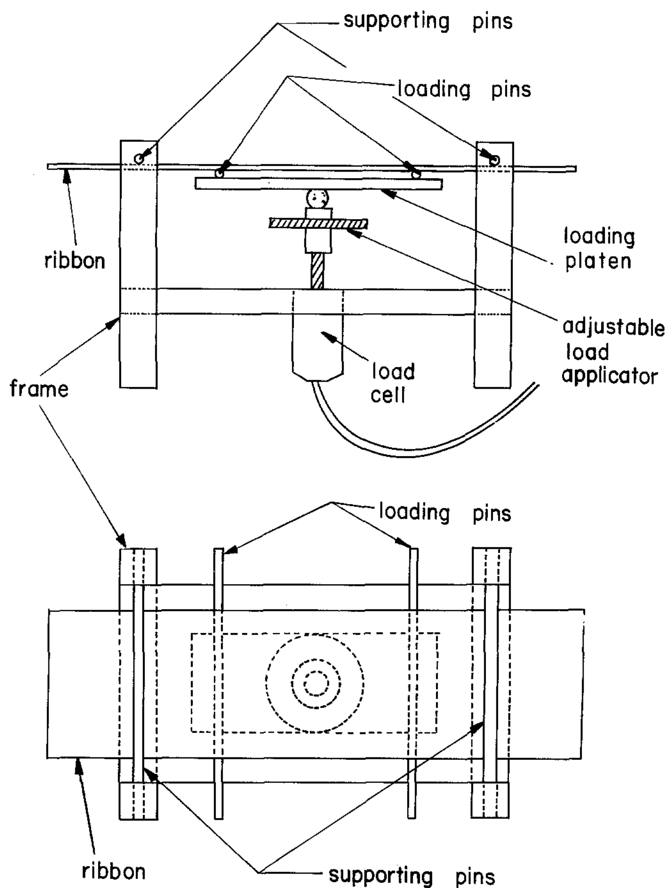

Figure 7 Schematic diagram of a four-point bend fixture used to flex a silicon plate by a specific applied load.

As can be seen from Equations 10 and 13, the curvature at any length along a deflected plate is dependent on M, the applied moment, and P, the stress residual. The determination of the curvature of a thin, short silicon plate is given below.

3. Experimental technique

A thin short rectangular plate of silicon is positioned in a four-point bend apparatus as shown in Fig. 7. This fixture, which is mounted on an optical bench, is used to flex the silicon with loads that are recorded by a load cell. An optical grating with 200 lines per in. (7874 per m) is positioned in front of the silicon and the silicon surface is illuminated by a helium–neon laser. A pattern of light and dark fringes can be seen if the silicon surface is viewed through the optical grating [10]. Fig. 8 shows a schematic diagram of the optical system, the four-point bend fixture and the camera used to record the fringe pattern as a function of load on the silicon. The interference fringes and the fringe density can be used to measure the out-of-plane displacements and the curvature.

Fig. 9 shows the interferogram obtained after deflection of the 0.03 cm × 10.2 cm × 5.1 cm silicon plate by a load of 2 N. To find the local curvature R of the silicon plate at an arbitrary Point Q, a three-point method is used in conjunction with the optical data in the vicinity of Point Q. Fig. 10 shows a small portion of the silicon plate which contains Point Q at which optical information is gathered.

The radius of curvature of the silicon plate at Point Q is obtained by passing a circle through the data points. The circle has the functional form

$$x^2 + z^2 + 2dx + 2ez + f = 0 \quad (14)$$

the radius of which can be expressed as

$$R = (d^2 + e^2 - f)^{1/2} \quad (15)$$

where d, e, and f are constants to be determined.

After reducing the optical information at three solution stations surrounding Point Q, we get (x_1, z_1) at Point 1, (x_2, z_2) at Point 2 and (x_3, z_3) at Point 3. Substituting these data into Equation 14, we get

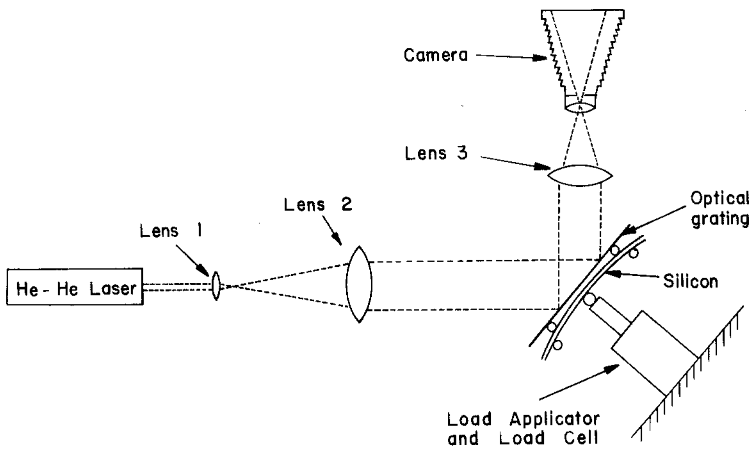

Figure 8 Schematic diagram of the optical system.

$$2dx_1 + 2ez_1 + f = -(x_1^2 + z_1^2)$$
$$2dx_2 + 2ez_2 + f = -(x_2^2 + z_2^2)$$
$$2dx_3 + 2ez_3 + f = -(x_3^2 + z_3^2)$$

or in matrix form

$$\begin{bmatrix} x_1 & z_1 & 1 \\ x_2 & z_2 & 1 \\ x_3 & z_3 & 1 \end{bmatrix} \begin{matrix} 2d \\ 2e \\ f \end{matrix} = -\begin{bmatrix} x_1^2 + z_1^2 \\ x_2^2 + z_2^2 \\ x_3^2 + z_3^2 \end{bmatrix}$$

from which d, e and f can be calculated to determine the local radius R. The reciprocal of this radius is equal to $2A$ and since M and w are known, Equations 10 and 13 may be used to obtain P.

4. Application to polycrystalline silicon sheet

The shadow Moiré technique for measurement of residual strains and the analysis above have been applied to thin flat plates of polycrystalline silicon ribbon grown by edge-defined film growth (EPG) technique into long ribbons 10 cm wide × 0.05 mm thick × L, and sectioned into 15 cm long strips. These strips, used in solar cell manufacture, have surfaces that replicate the graphite dyes through which the ribbon is extracted and the thickness uniformity is ~15% [11]. A representative interferogram of a 10.2 cm long ribbon that had been grown at 2 cm min^{-1} is shown in Fig. 9. This figure shows the non-uniform fringe pattern representative of a complex surface geometry and residual stress distribution. The residual stresses along the length have been determined from this interferogram and the results are shown in Fig. 11. This figure shows σ_{xx} at 0.5, 1, 2, 3 and 3.5 in. (12.7, 25.4, 50.8, 76.2 and 88.9 mm) from one end of the ribbon. As can be seen, the residual stress is tensile in the centre and compressive at the edges, the maximum stresses having a magnitude of 7 MPa.

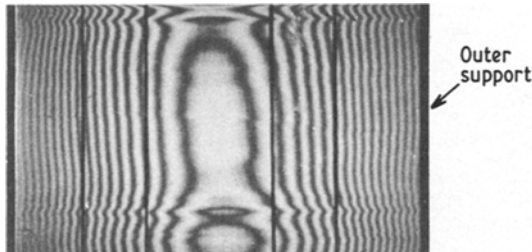

Figure 9 Shadow Moiré interferogram of a thin short silicon plate flexed in a four-point bend fixture with a load of 2 N.

Acknowledgements

The initial stages of this work were supported by the Mobil Solar Energy Corporation and continuing support was provided by the Jet Propulsion Laboratory, Flat-Plate Solar Array Project No. 956053. This support is gratefully acknowledged. Dr J. Kalejs of Mobil Solar Energy Corporation and Dr A. Morrison of the Jet Propulsion Laboratory provided much-needed

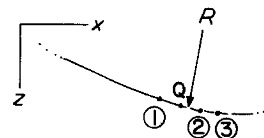

Figure 10 Schematic diagram of the geometry of the local curvature of the silicon plate.

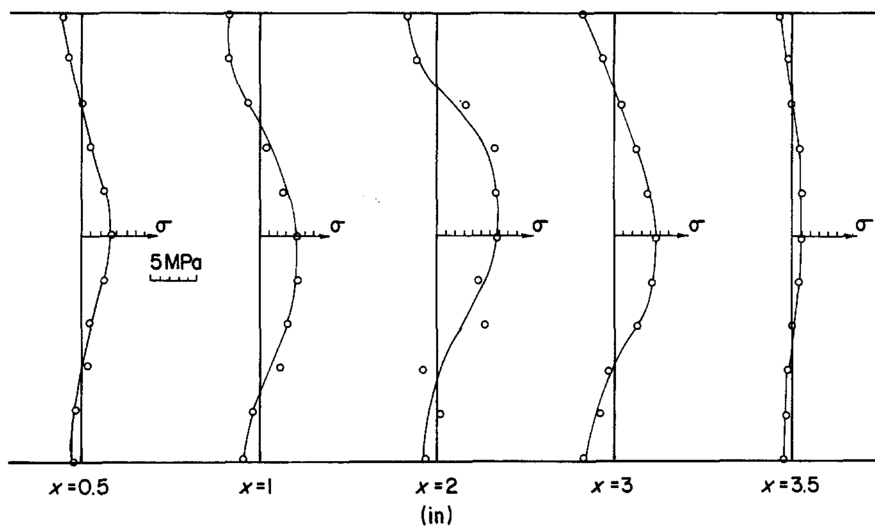

Figure 11 Residual stress distribution at various distances from the left end of a silicon EFG ribbon.

encouragement throughout the course of this work. Dr C. P. Chen of JPL contributed to the successful completion of this work. We appreciate the technical discussions with Drs B. Wada and C. Hsieh of JPL and Professor J. Hutchinson of Harvard University.

References

1. J. T. NORTON, *Mater. Evaluation* **31** (1973) 21.
2. M. JAMES and J. B. COHEN, *ASTM J. Testing and Evaluation* **6** (2) (1978) 91.
3. R. G. BATHGATE, *Strain J. Br. Soc. Strain Measmt* **4** (2) (1968) 20.
4. H. FUKUOKA, H. TODA and H. NAKA, *Exp. Mech.* **23** (11) (1983) 120.
5. V. VILHELMY and H. KUBLER, *Proc. Soc. Expl. Stress Analysis* **30** (1) (1973) 142.
6. J. H. UNDERWOOD, *ibid.* **30** (2) (1973) 373.
7. N. TEBEDGE, G. ALPSTEN and L. TALL, *ibid.* **30** (1) (1973) 88.
8. A. S. KOBAYASHI (editor), "Experimental Techniques in Fracture mechanics", Society for Experimental Stress Analysis Monograph No. 2 (Iowa State University Press and Society for Experimental Stress Analysis, Westport, Connecticut, 1975) p. 59.
9. C. M. VEST, "Holographic Interferometry" (John Wiley, New York, 1979).
10. A. ANDONIAN and S. DANYLUK, *Mech. Res. Commun.* **11** (2) (1984) 97.
11. F. V. WALD, *Crystals, Growth Properties & Applns* **5** (1981) 1.

Received 28 December 1984
and accepted 16 January 1985